International Journal of Maritime Technology

Hydrodynamic Performance Analysis of Modular Chain-Type Floating Docks for High-Speed Boat Operations in Semi-Enclosed Port Basins: A Multi-Body Simulation Approach using ANSYS AQWA

Seyed Reza Samaei [1] iD **, Mohammad Asadian Ghahfarokhi** [2]* iD

1- Assistant professor, Department of Civil Engineering, SR.C., Islamic Azad University, Tehran, Iran; samaei@srbiau.ac.ir
2- Assistant professor, Department of Civil Engineering, SR.C., Islamic Azad University, Tehran, Iran; asadian@srbiau.ac.ir

ARTICLE INFO	ABSTRACT
	This study investigates the hydrodynamic performance of modular, chain-type floating docks designed for high-speed boat deployment within the operational zone of Shahid Bahonar Port. Given the limitations of fixed dock infrastructure—particularly in regions with soft seabeds and tidal variations—floating docks offer a flexible, cost-effective alternative. A modular pontoon system was designed using CATIA and analyzed in ANSYS AQWA under various wave conditions (0°, 45°, 90°, 135°, and 180°). Comparative simulations between single-body and multi-body configurations revealed that multi-hull docks significantly reduce vertical displacement and better distribute wave-induced forces, especially at connection points. Time-domain analyses further confirmed that joint stiffness and orientation strongly influence structural response. Elastic mooring systems enhanced the dock's adaptability to dynamic sea conditions while minimizing environmental impact. These findings support the development of resilient floating marine structures tailored to the hydrodynamic conditions of semi-enclosed ports like Shahid Bahonar, with implications for both defense and commercial applications in high-salinity environments.

1. Introduction

Research on large floating structures has advanced globally, supporting applications such as breakwaters, airports, terminals, and docks. Floating docks, introduced in industrialized nations in the mid-20th century, remain an emerging field in coastal and port engineering. In Iran, their development is limited, with little practical expertise, as existing structures, like the Amirabad Floating Dock, are primarily foreign-made with restricted design and construction data. This study examines the hydrodynamic behavior of chain-type floating docks and parking structures for high-speed boat deployment within the operational range of Shahid Bahonar Port. Given the high cost and time investment of fixed docks and breakwaters, the maritime industry increasingly favors floating alternatives. These docks, constructed from materials such as composite, aluminum, steel, and polywood, facilitate cargo handling and vessel mooring, particularly in regions with extreme tidal variations and offshore environments. Their stable surface level makes them suitable for vehicle, passenger, and equipment transportation, while also serving as docking and service stations for various vessel sizes. This study focuses on composite floating docks, chosen for their strength, efficiency, and corrosion resistance—a critical factor in marine environments. The GRP composite coating enhances structural durability and prevents moisture penetration, with resins and topcoats specifically designed for UV and marine resistance. Additionally, pontoons, waveguides, and dock fingers are built from highly chemical-resistant materials to ensure longevity. To minimize environmental impact, particularly in the high-salinity Persian Gulf, pontoons are surfaced with composite wood, a durable, low-maintenance blend of wood and polyethylene that withstands harsh conditions, moisture, and seawater while retaining the aesthetics of natural wood.

Fig. 1. Example of Floating Dock and Parking Structures for Mooring

2. Methodology

Due to the complexities associated with mathematical modeling of hydrodynamic interactions in multi-body structures, utilizing specialized software for hydrodynamic analysis is a practical approach. In this study, the design of pontoon structures is initially determined using theoretical and standard equations to define their dimensions. Next, CATIA P3 V5-6R2016 is used to generate detailed structural drawings of the pontoons and their connections, which serve as inputs for subsequent simulations. The floating docks are then modeled as rigid-body structures with articulated connections in ANSYS AQWA, where structural and hydrodynamic analyses are conducted under wave loads. These simulations evaluate the structural response of the system, incorporating essential inter-body connections and hydrodynamic forces.

2.1 Structure of Floating Docks

Floating docks are constructed from various materials, including metal, wood, and composite, depending on their intended use and environmental conditions. Among these, composite docks are widely utilized due to their strength, durability, and corrosion resistance. These docks typically consist of resin-reinforced fiberglass (FRP) with a structural framework of reinforced concrete, metal, composite, or a combination of these materials. Their composition is selected based on operational requirements and environmental constraints. The following figure illustrates an example of such floating docks.
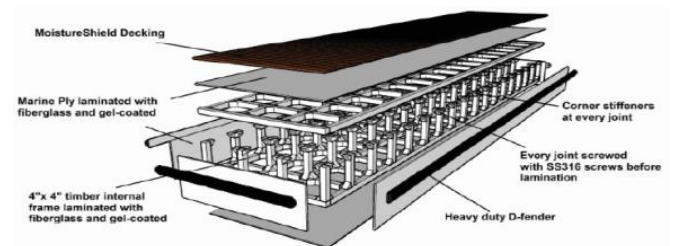

Fig. 2. Schematic view of a composite floating dock [2]

2.2 Mooring and Connection of Floating Structures

Floating structures, whether used as floating bridges or offshore docks, require secure mooring to maintain stability. When positioned away from the shore, individual floating units are anchored to the seabed using high-resilience elastic mooring cables, selected based on engineering standards and minimum stress requirements. For nearshore floating docks, mooring is achieved through one or more floating bridges, which provide a connection to the shore. These connections may be rigid or articulated, depending on design specifications, and must account for tidal variations and currents. Ramps are typically used in shore connections to accommodate vertical oscillations, ensuring smooth access under fluctuating water levels. The connection method, structure type, and length depend on site-specific conditions, regional constraints, and the dock's intended function. If a floating bridge is utilized as a connector, it can be stabilized using mooring cables and

anchors or by pile-driving at both ends to enhance stability and operational efficiency in varying marine environments.

Fig. 3. A view of the access bridge to the composite floating dock

2.3 Mooring Methods for Floating Docks

For floating docks positioned near the shore, mooring using cables and anchors is essential to ensure stability. Two main types of anchors are employed based on water depth and seabed conditions. Type A anchors are used in deep waters with soft seabeds, consisting of reinforced concrete units that are embedded into the seabed using water jets, allowing them to penetrate mud and sediment for a secure hold. Their capacity depends on seabed resistance, sediment pressure, and soil composition. In contrast, Type D anchors are designed for deep waters with hard seabeds and high strength requirements. These heavily reinforced concrete anchors, constructed in a layered stone-like manner, are chosen based on the floating structure's dimensions and regional aquatic conditions. The most efficient and environmentally friendly mooring method for floating docks combines anchors with elastic ropes, eliminating the need for pile driving and seabed foundations. These elastic mooring systems effectively adapt to tidal fluctuations, preventing excessive movement while ensuring long-term stability. Spiral anchors, known for their high corrosion resistance and tensile strength, further enhance durability due to their helical structure.

1. Advantages of Elastic Mooring Systems:

2. Minimizes prolonged and severe fluctuations of the floating dock.

3. Enhances stability by securing the dock to the seabed through elastic cables connected at multiple points.

4. Ensures high chemical and tensile resistance, preventing degradation over time.

5. Offers excellent fatigue resistance, allowing the dock to remain securely in place for extended periods.

This mooring approach provides a sustainable, resilient, and adaptive solution for floating docks, ensuring stability while reducing environmental impact.
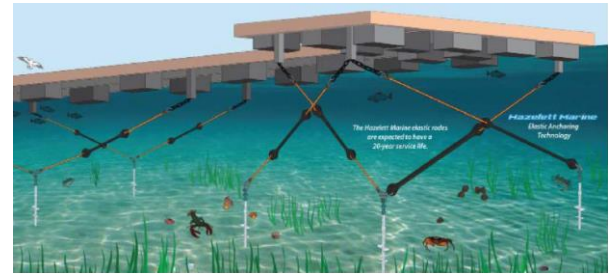

Fig. 4. Schematic Representation of Composite Floating Dock Mooring [2]

2.4 Definition of a Floating Craft Suitable for a Passenger Floating Dock

The selection of a suitable floating craft for berthing at a passenger floating dock is determined based on key operational and structural parameters. As referenced in [1], the criteria for identifying the appropriate vessel type can be derived from Table 1, which outlines essential specifications such as dimensions, displacement, draft, and berthing requirements. These factors ensure compatibility between the floating dock and the vessels it accommodates, optimizing safety, efficiency, and stability in docking operations.

Table. 1. presents the specifications of a sample passenger ferry craft [1]

Craft Name	Length (meters)	Width (meters)	Draft (meters)	Passenger Capacity
Azarkhosh	9.14	4.5	4.1	63

2.5 Characteristics of a Passenger Floating Dock

The length and number of floating docks are directly influenced by passenger traffic and cargo transportation demands. The total dock length (LB) is determined using the following formula:

$$LB=L+d \qquad (1)$$

Where:

- LB is the average berthing length.

- L is the average ship length.

- d is the distance between ships.

For docks accommodating multiple vessels, the value of d can be obtained from Table 2, which provides standard clearance distances based on ship length. This calculation ensures efficient space utilization, safe

berthing operations, and optimized passenger flow management at the floating dock.

Table. 2. Distance Between Ships at the Dock [2]

Average Ship Length (m)	<100	100−149	150−200	>200
d		10	15	20	25

The width of the floating dock is determined based on the transportation equipment used on it and whether it allows berthing on one or both sides.

The minimum required depth in a floating dock can be calculated using the following relationship [3].

$$D = d + Z_1 + Z_2 + Z_3 + Z_4 + Z_5 \qquad (2)$$

Where:

- D is the minimum required depth for design.

- d is the draft at maximum ship loading at zero speed.

- Z_1 is the freeboard distance of the ship's bottom to create a safety margin against bottom collision, typically taken as a minimum of 0.5 meters. In conditions of severe damage, such as in ports with rocky bottoms, this value may increase to one meter.

- Z_2 is the vertical ship oscillation range against waves caused by wind, where $Z_2=0.5×HW$ $Z_2=0.5×HW$ (where HW HW is the wave height at the dock).

- Z_3 is the allowable angle of ship rotation, $Z_3=K×VS$, where VS is the ship's speed during berthing or departure. For medium and large ships, VS is very low, and Z_3 is typically zero.

- Z_4 is the potential sediment accumulation between two dredging stages in the basin, and Z_5 is the necessary tolerance for dredging operations; typically ranging from 0.3 to 2.5 meters.

The depth of a harbor should be measured from the lowest level (LW) or the mean of the tidal range (MLWS). Since selecting a reference water level is often prone to error, the depth of water at a floating dock in a protected harbor can be assumed to be up to ten times the draft of the largest ship [4].

2.6 Statistical Information of Shahid Bahonar Port

Shahid Bahonar Port, one of the oldest multipurpose ports in Hormozgan province, is a key hub for non-oil exports, cargo transportation, and passenger transit in Iran. As the third-largest export port in the country, it holds a strategic position due to its proximity to international waters via the Persian Gulf, connectivity to global shipping routes, and access to commercial hubs such as Qeshm Free Zone and other Persian Gulf ports. Following Shahid Rajaee Port Complex, it serves as a critical maritime base for trade and transport. A distinguishing feature of Shahid Bahonar Port is its 10.2-meter draft at full tide, making it the deepest port in the country after Imam Khomeini Port and Shahid Rajaee Port. Historically, it was the primary port of Bandar Abbas and continues to accommodate a high volume of passengers and tourists daily due to its central location within the city. A significant portion of Bandar Abbas' commercial activity relies on this port, reinforcing its role in the region's economic development. The following section presents seasonal wave patterns in the Persian Gulf and the Sea of Oman, relevant to this study. The wave characteristics used in the numerical simulations were selected based on historical oceanographic data specific to the Persian Gulf and Shahid Bahonar Port, as illustrated in Figure 5. These include regular waves with amplitudes ranging from 0.3 to 1.0 meters and frequencies between 0.148 and 0.288 Hz, chosen to reflect both typical and extreme wave conditions in semi-enclosed port basins.
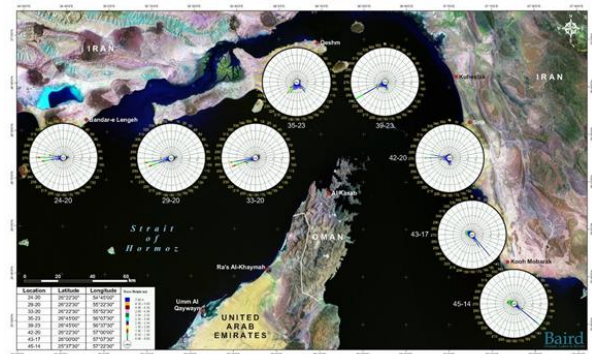

Fig. 5. Seasonal Wave Patterns of Southern Iranian Ports

2.7 Hydrodynamic Analysis and Numerical Simulation of Floating Docks

Extensive research has been conducted on the hydrodynamic behavior of floating structures, employing various computational methods and software tools. Tajali utilized MOSES software to analyze wave diffraction and radiation effects, estimating hydrodynamic forces and their impact on floating structures [64]. Hanif applied the finite element method to examine the hydrodynamic response of floating breakwaters in heave and sway motions [15]. Similarly, Satio and Kubo used boundary integral equations to determine the motion characteristics of two interconnected floating docks under regular wave conditions [16]. Other studies, including those by Lee et al. [17], Wang and Ohkusu

[18-20], and Choi & Hong [25], investigated wave interactions with multi-body floating systems using numerical and analytical approaches. The role of incident wave direction in motion response has been widely studied, with researchers such as Isaacson and Nwogu [32] proposing wave force reduction factors to optimize floating structure orientation. Most floating docks and breakwaters experience random, wind-generated waves with relatively low wave heights, resulting in moderate hydrodynamic loads [34]. Hutchinson analyzed frequency domain responses of floating breakwaters under short waves, identifying the effects on six degrees of freedom, including pitch motion and induced moments [35]. Given that large floating structures often consist of multiple interconnected modules, hydroelastic analysis has been widely applied to assess structural movements and response under wave action. Studies by Wang et al. [36], Che et al. [37], and Riggs & Ertekin [40] have refined multi-body hydrodynamic interaction models to improve computational efficiency, reducing complexity through rigid and flexible connection modeling.

1. Modeling and Numerical Simulation of Floating Docks

In this study, ANSYS AQWA is utilized for the numerical investigation of floating dock performance, due to its comprehensive hydrodynamic modeling capabilities. The hydrodynamic response of the floating dock was modeled using three-dimensional linear diffraction theory, which solves the potential flow equations in the frequency domain. This method accounts for wave-body interactions in all six degrees of freedom (surge, sway, heave, roll, pitch, and yaw), making it suitable for analyzing complex floating structures with multiple interconnected modules. The software is widely used for analyzing wave, wind, and current effects on floating marine structures, including floating docks, oil platforms, semi-submersibles, ships, and renewable energy systems [Samaei et al., 2021]. The modeling approach was validated based on the previously published work by Samaei et al. (2016), in which numerical results using ANSYS AQWA were compared with laboratory experimental data for a similar pontoon structure, demonstrating strong agreement. Its advanced modeling features contribute to cost reduction and time efficiency in floating structure design [Samaei et al., 2016].

The single-hull model was created by rigidly connecting all pontoons along their full contact length, forming a continuous monolithic floating platform with a total length of 30 meters. Unlike the articulated joints used in the multi-hull model, this configuration assumes zero flexibility, simulating a rigid-body response to wave loads.

2. Modeling a Floating Dock in ANSYS AQWA

The modeling process consists of two primary stages:

3. Creating the geometry of the floating dock.

4. Defining hydrodynamic conditions and performing wave interaction analysis in the Hydrodynamic Diffraction module.

Two methods are available for generating the dock model: (1) importing a pre-designed geometry from CATIA, or (2) constructing the model directly within ANSYS AQWA's Model Designer using curved and non-curved panels and Morrison elements (e.g., tubes, stubs, and discs) [Samaei et al., 2022]. In this study, CATIA was used to develop the structural model, incorporating detailed engineering elements such as connections, fenders, mooring components, and material specifications, as illustrated in the figures below [Samaei et al., 2021].

- Access Bridge: This bridge measures 12m * 1.5m and is made of aluminum AL 6005. Its surface is covered with blast wood, and its gangway is connected to a concrete pad on the shore.
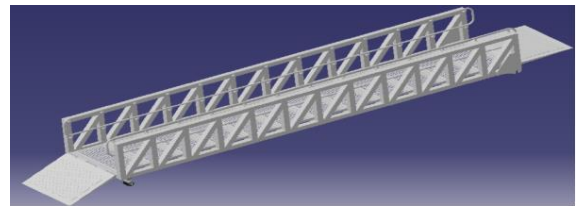

Fig. 6. 3D View of the Access Bridge to the Floating Dock

- Piles and Mooring: The dock is equipped with 18 moorings, each capable of supporting 5 tons.
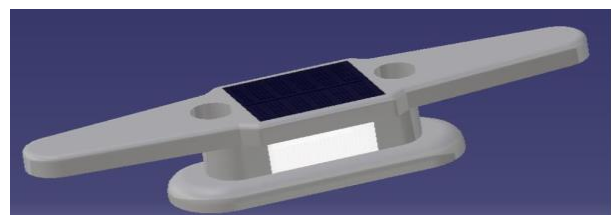

Fig. 7. View of the Mooring and Bollard on the Floating Dock

- Fenders: Fenders with a cross-sectional area of D are considered to cover 100% of the total surface area of the dock structure walls.
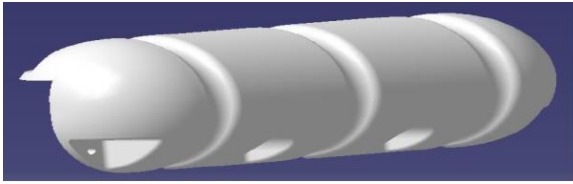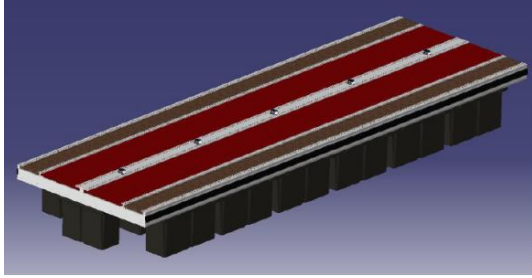
Fig. 8. 3D View of the Fender on the Floating Dock

- Main Pontoon: The main pontoon measures 3m * 1m and is made of aluminum AL 6005. Its surface is covered with blast wood, and its gangway is connected to a concrete pad on the shore.

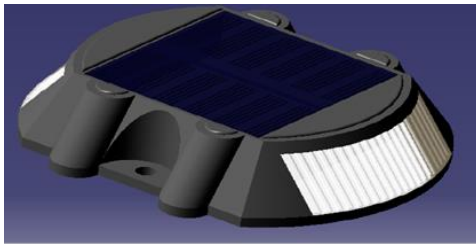**Fig. 9. 3D View of the Main Pontoon on the Floating Dock**

• Lighting fixtures

Fig. 10. 3D View of the Lighting Fixture on the Floating Dock

Final Design of the Dock and Floating Parking Lots: Dimensions (Length * Width) 30m * 3m Total buoyancy: 700 kg/m2 and Freeboard: 1m the connection between pontoons should be capable of bearing a load of 20 tons. The connection method is mooring, with 6 connections from stainless steel 316L embedded in the floor.
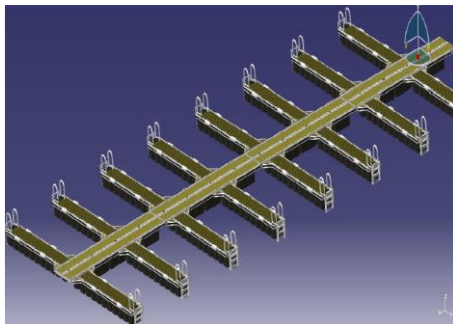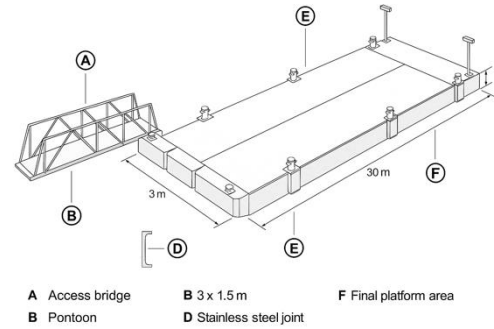

Fig. 11. 3D View of the Final Design of the Dock and Floating Parking Lots

The connection between pontoons should be capable of bearing a load of 20 tons. The connection method is mooring, with 6 connections from stainless steel 316L embedded in the floor.

A Access bridge   B 3 x 1.5 m   F Final platform area
B Pontoon   D Stainless steel joint

Fig12 a). Integrated Schematic of Floating Dock System Components

This figure provides a comprehensive isometric schematic of the modular floating dock system. Key elements include the access bridge (A), pontoons (B), stainless steel joints (D), mooring points (C), fenders and platform features (E), and lighting fixtures (F). The layout is based on the geometric data and structural design presented in Figures 6 through 11.

2.8 Multi-Component Model

In this model, the overall geometry of the dock is represented as a combination of pontoons, each of which is connected to the others through articulated joints. The figure below illustrates 8 distinct sections of the dock that have been highlighted for hydrodynamic analyses.
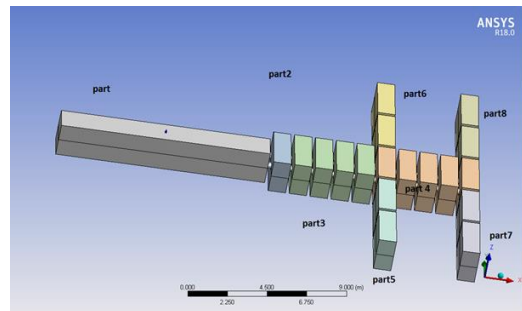

Fig. 12 b). Multi-Component Model of the Floating Dock in the Model Designer Section of ANSYS AQWA

In the figure below, all defined connections for solving in the time domain are illustrated. The dock's connection set includes a rigid connection between the bridge and the concrete platform, as well as arms that provide one degree of freedom between the pontoons.
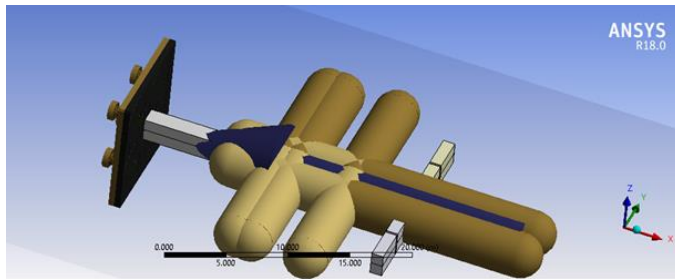
Fig. 13. Representation of the Defined Connections for the Multi-Component Dock Structure Model

2.9 Meshing and Grid Generation in ANSYS AQWA Software

In this study, default settings available in the software have been utilized for meshing the structure. The specifications, sizes, numbers, etc., of meshes and nodes are provided in the tables below.

Table. 3. Specifications of Meshes Used in Hydrodynamic Analysis of the Sample Floating Dock Model

NAME	MESH
STATE	MESHED
DETAILS OF MESH	
DEFAULTS	
CONTROL TYPE	BASIC CONTROLS
MESH PARAMETERS	
DEFEATURING TOLERANCE	2 m
MAXIMUM ELEMENT SIZE	5 m
MAXIMUM ALLOWED FREQUENCY	0.603 Hz
MESHING TYPE	PROGRAM CONTROLLED
GENERATED MESH INFORMATION	
NUMBER OF NODES	2716
NUMBER OF ELEMENTS	2834
NUMBER OF DIFFRACTING NODES	1588
NUMBER OF DIFFRACTING ELEMENTS	1424
NUMBER OF FIELD POINTS	0
NAME	MESH SIZING
STATE	FULLY DEFINED
DETAILS OF MESH SIZING	
ACTIVITY	NOT SUPPRESSED
SELECT GEOMETRY	266 BODIES
LOCAL ELEMENT SIZE	1 m

In the modeling of the floating dock investigated in this research, a drag coefficient and added mass coefficient of 1 have been assumed. The fluid density is set to 1025 kg/m³. Meshing for structures has been performed with minimum conditions of 3 mm and maximum conditions of 3 cm. Below is an illustration of the completed model of the pontoon floating dock.

The hydrodynamic analysis conducted in this study is based on the principles of potential flow theory, assuming an incompressible, inviscid, and irrotational fluid. The governing equation is the Laplace equation for the velocity potential ϕ:

$$\nabla^2\phi=0$$

Subject to the following boundary conditions:

- **Free surface boundary condition**: Linearized to account for small-amplitude wave assumptions.

- **Body boundary condition**: No flow normal to the body surface.

- **Seabed boundary condition**: No vertical velocity at the bottom.

- **Radiation condition**: At infinity, outgoing waves are assumed.

ANSYS AQWA solves these equations using a boundary element method (BEM) and diffraction theory in the frequency domain. For time-domain simulations, response amplitude operators (RAOs) are used as input to derive motion responses under transient wave loading.

The computational domain was defined large enough to minimize boundary reflections and numerical instabilities. The boundaries extend at least one full wavelength in all directions from the floating dock structure. ANSYS AQWA applies an absorbing boundary condition at the domain edges to simulate open-sea conditions. This ensures that incident and diffracted waves are properly resolved without interference from artificial boundary reflections.
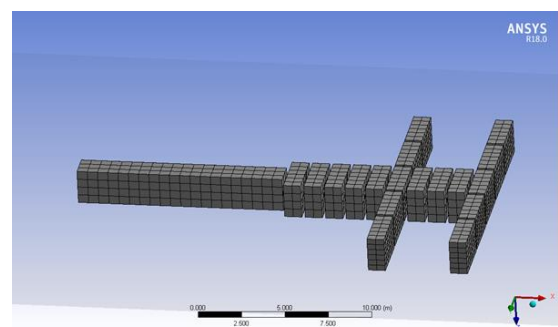

Fig. 14. Representation of the Generated Mesh for Interaction Analysis in ANSYS AQWA Software

52

A mesh sensitivity analysis was performed to ensure convergence and solution accuracy. Several mesh configurations were tested, including finer and coarser elements, and the resulting motion amplitudes and wave forces were compared. The differences in vertical displacement and force values were found to be less than 3% between the selected mesh and a finer one, confirming mesh independence. Therefore, the adopted mesh settings (maximum element size = 5 m, local element size = 1 m) offer a balance between computational efficiency and accuracy.

This study examines the hydrodynamic behavior of both a single-body floating dock and a multi-pontoon chain of constant 30-meter length under wave incidences at 0°, 45°, 90°, 135°, and 180°. For the multi-pontoon configuration, pontoons are interconnected using hinge joints positioned at the pontoon's width level and 30 cm above it. In contrast, the single-body configuration features pontoons rigidly connected, treating the dock as a rigid floating structure.

2.10 The ANSYS AQWA simulations include two key sections:

The floating dock is initially modeled as a single integrated structure and subjected to head-on waves (180° incidence angle). To ensure consistency in modeling, all pontoon connection points are assumed to be rigid connections within the software. The wave incidence direction on the structure is illustrated in the figure below.
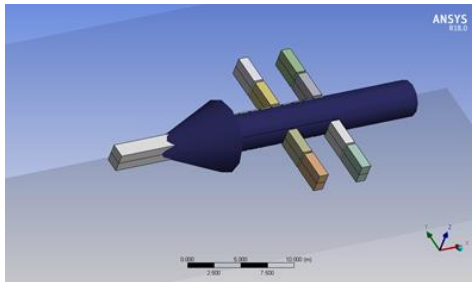

Fig. 15. Direction of Regular Wave Incidence (180 Degrees) to the Integrated Dock Model

The results of the analysis of the integrated model under regular wave incidence (180 degrees) are presented in the following figures and table.
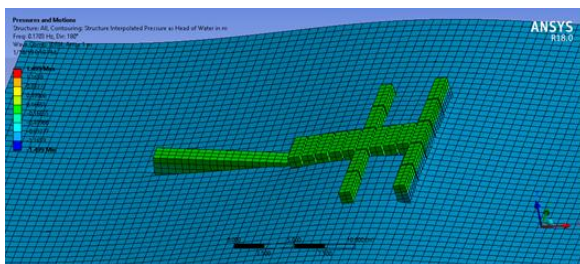

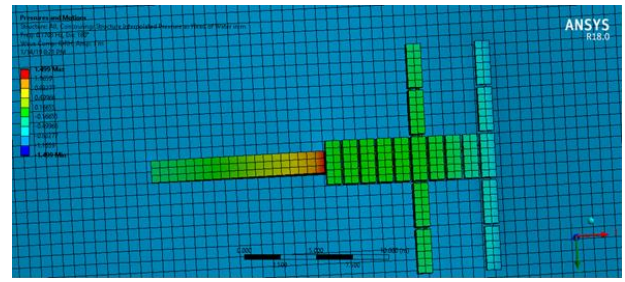**Fig. 16. Vertical Displacement of the Integrated Dock Model under Regular Wave Incidence (180 Degrees)**

Fig. 17. Pressure Contours and Displacement of the Integrated Dock Model under Regular Wave Incidence (180 Degrees)

Table. 4. Wave Specifications and Vertical Displacement Changes of the Integrated Floating Dock Model

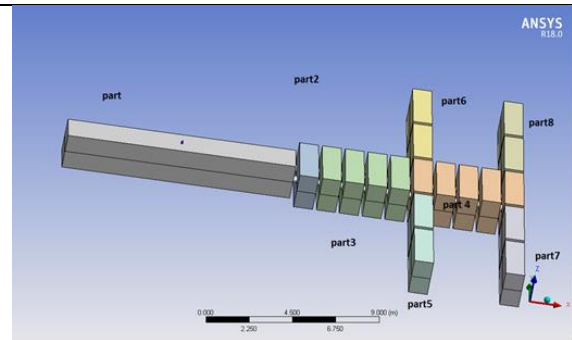| Wave Type	Wave Amplitude	Wave Frequency	Wave Direction	Maximum and Minimum Vertical Displacement of the Floating Dock
Regular	1 m	0.17 Hz	180°	1.499 m

Fig. 18. Definitions of Parts of the Floating Dock Model for Identifying Connection Points

Subsequently, the hydrodynamic diffraction analyses related to the chain-type floating dock encountering waves with incident angles of 0, 45, 90, 135, and 180 degrees are presented. A noteworthy point in these analyses is the vertical displacement of the dock and its arms, which will be discussed in detail in the following sections regarding the forces applied to the structure and connections.

The figures below depict the output of the diffraction analysis software for the multi-section dock model facing a 0-degree incident wave.
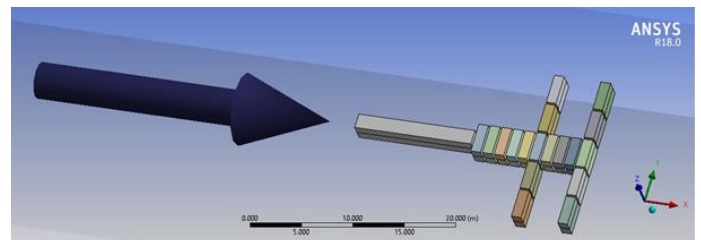

Fig. 19. Multi-Section Dock Model Facing a 0-Degree Incident Wave

Since floating docks are typically installed in calm basin areas and connected to the shore via access

53

bridges, the likelihood of direct encounter with 0-degree incident waves is very low, and these waves can be considered as reflective waves.
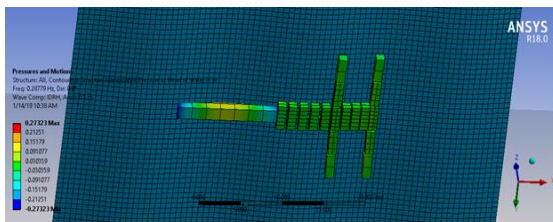

Fig. 20. Results of Diffraction Analysis for the Multi-Section Dock Model Facing a 0-Degree Incident Wave

The specifications of wave characteristics and vertical displacement changes of a multi-section floating dock model encountering zero-degree waves are presented in Table 5.

Table. 5. Wave Characteristics and Vertical Displacement Changes of a Sample Multi-Section Floating Dock Model

Wave Type	Wave Amplitude	Wave Frequency	Wave Direction	Maximum and Minimum Vertical Displacement of Floating Dock
Regular	0.3 m	0.288 Hz	0°	0.273 m, -0.273 m

The figures below depict the output of diffraction analysis software for a multi-section dock model encountering 45-degree waves.
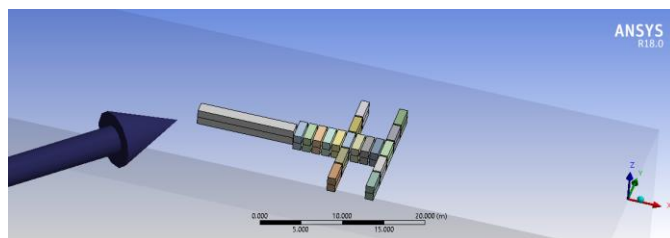

Fig. 21. Multi-Section Floating Dock Model Facing 45-Degree Waves
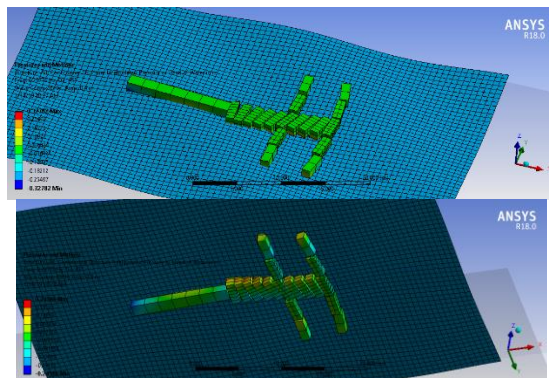

Fig. 22. Diffraction Analysis Results for a Multi-Section Dock Model Facing 45-Degree Waves

The figures below depict the output of diffraction analysis software for a multi-section dock model encountering 90-degree waves.
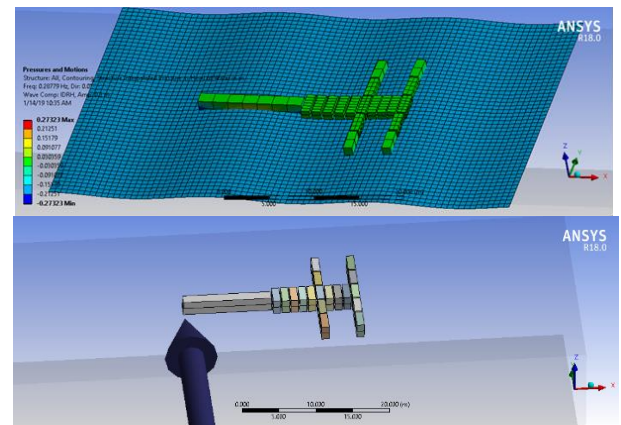

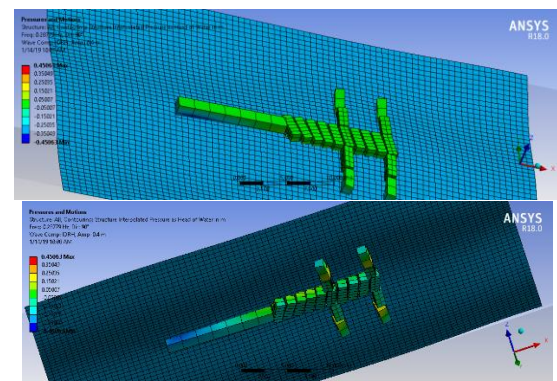**Fig. 23. Multi-Section Dock Model Facing 90-Degree Waves**

Fig. 24. Diffraction Analysis Results for a Multi-Section Dock Model Facing 90-Degree Waves

The figures below depict the output of diffraction analysis software for a multi-section dock model encountering 135-degree waves.
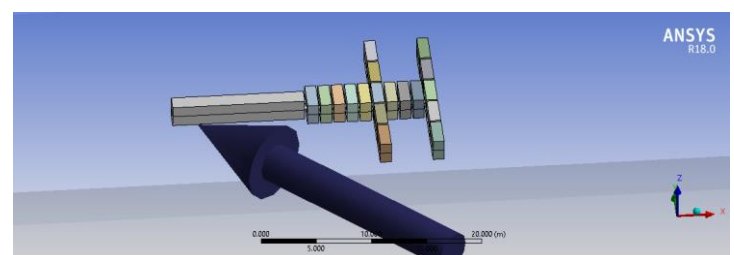

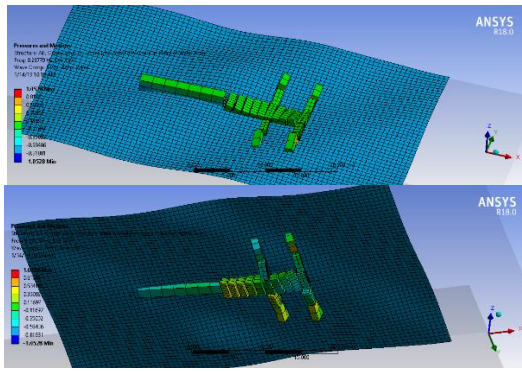**Fig. 25. Multi-Section Dock Model Facing 135-Degree Waves**

54

Fig. 26. Diffraction Analysis Results for a Multi-Section Dock Model Facing 135-Degree Waves
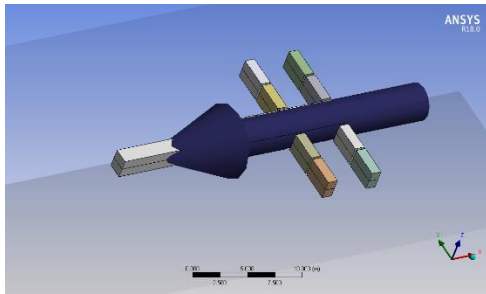

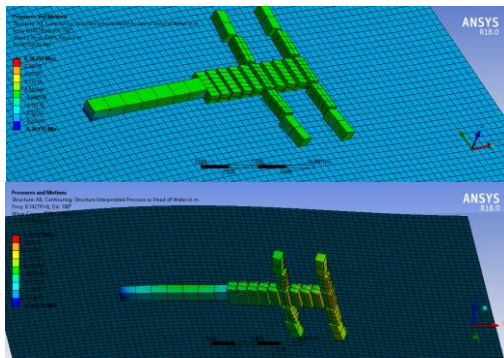**Fig. 27. Multi-Section Model Encountering 180-Degree Waves**

Fig. 28. Diffraction Analysis Results for a Multi-Section Dock Model Facing 180-Degree Waves

At the end of this section, for the purpose of comparing the vertical motions of single-hull and multi-hull floating docks in various wave conditions, the following table is provided:

Table. 6. Wave Characteristics and Vertical Displacement Changes of Single-Hull and Multi-Hull Floating Dock Models

Dock Type	Wave Type	Wave Amplitude	Wave Frequency	Wave Direction	Maximum and Minimum Vertical Displacement of Floating Dock
Single-Hull	Regular	1 m	0.17 Hz	180°	1.499 m, -1.499 m
Multi-Hull	Regular	0.3 m	0.288 Hz	0°	0.273 m, -0.273 m

Dock Type	Wave Type	Wave Amplitude	Wave Frequency	Wave Direction	Maximum and Minimum Vertical Displacement of Floating Dock
Multi-Hull	Regular	0.4 m	0.288 Hz	45°	0.328 m, -0.328 m
Multi-Hull	Regular	0.4 m	0.288 Hz	90°	0.451 m, -0.451 m
Multi-Hull	Regular	0.4 m	0.288 Hz	135°	1.053 m, -1.053 m
Multi-Hull	Regular	1 m	0.148 Hz	180°	0.364 m, -0.364 m

As evident in the presented results, multi-hull docks exhibit less vertical motion compared to single-hull docks, indicating a potentially better operational performance in encountering collision waves.

2.11 Hydrodynamic Time Response Analysis

This section examines the forces acting on the floating dock structure and its connections under different wave conditions. To accurately model these interactions, the locations and types of connections must first be defined in the simulation software.

As detailed in previous sections, a solid (rigid) connection is applied at the junction between the access bridge and the shore, while a hinged connection is used on the opposite side. The first pontoon is connected via hinges to the following four-pontoon section, which is treated as a rigid unit. This pattern is repeated throughout the dock, ensuring structural consistency. Additionally, each lateral arm is attached to the main structure through hinged connections, allowing for controlled movement and flexibility under wave forces.

The diagram below illustrates the designated connection points and different structural areas considered in the floating dock model.
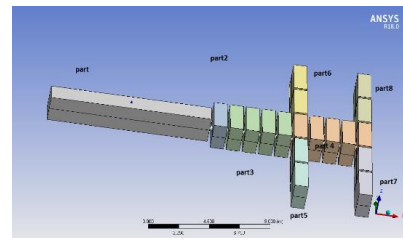

Fig. 29. An overview of the multi-hull dock structure in the Time Response solution.

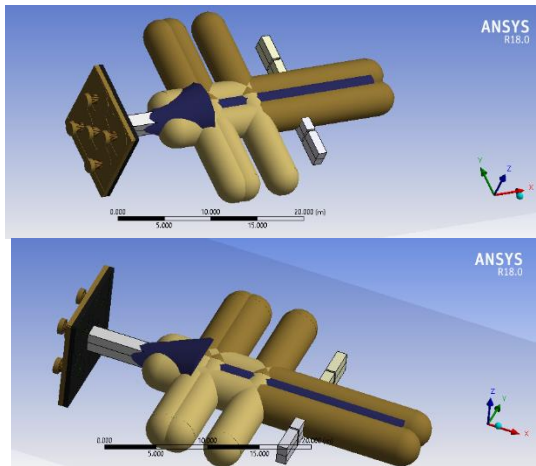In the figures below, the locations of the joints are indicated.

Fig. 30. A view of the connection's definition in the Time Response solution.

In this section of the research, after considering the joint locations, the forces acting on each point of the multi-hull dock structure are analyzed using the input data from Table 4-3 as the wave loads. The results of the analysis of the forces acting on the dock structure and its joints when confronted with a 45-degree incident wave are presented in the figures below.
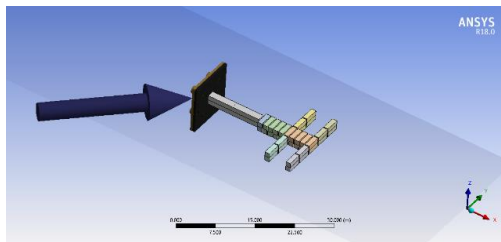

Fig. 31. A depiction of the 45-degree angle wave collision with the multi-hull floating dock in the Time Response solution.

In the figure below, the forces acting on joints 1 to 4 during the collision of a 45-degree angle wave with the multi-hull floating dock in the Time Response solution are depicted.

Fig. 33. The force applied to joints 1 to 4 during the collision of a 45-degree angle wave with the multi-hull floating dock in the Time Response solution.

In the figure below, the forces acting on joints 5 to 8 during the collision of a 45-degree angle wave with

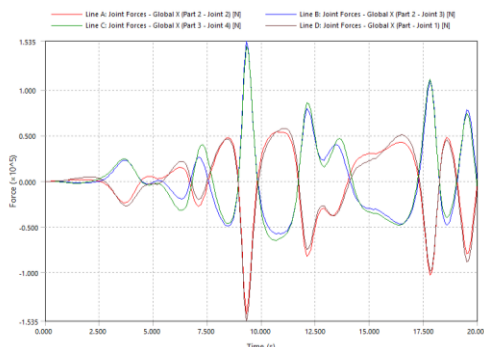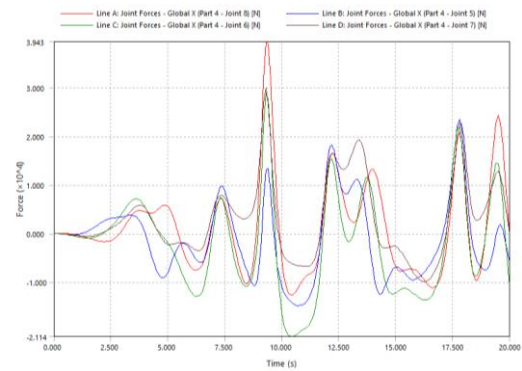the multi-hull floating dock in the Time Response solution are depicted.

Fig. 34. The force applied to joints 5 to 8 during the collision of a 45-degree angle wave with the multi-hull floating dock in the Time Response solution.

As observed in the above figures, in this situation, the highest forces are applied to joints 1 to 4 at the connection points of the initial sections of the dock. In other words, due to the presence of fixed supports at the beginning of the dock, the forces are more concentrated on these parts, increasing the likelihood of damage at these points of the structure.

The results of the analysis of the forces acting on the dock structure and its joints when confronted with a 90-degree incident wave are presented in the figures below.

Fig. 35. A depiction of the 90-degree angle wave collision with the multi-hull floating dock in the Time Response solution.

Fig. 36. The force applied to joints 1 to 4 during the collision of a 90-degree angle wave with the multi-hull floating dock in the Time Response solution.

56

Fig. 37. The force applied to joints 5 to 8 during the collision of a 90-degree angle wave with the multi-hull floating dock in the Time Response solution.

As observed in the above figures, in this situation, the highest forces are applied to joints 1 and 2 at the connection points of sections 1 and 2 of the dock. The results of the analysis of the forces acting on the dock structure and its joints when confronted with a 135-degree incident wave are presented in the figures below.
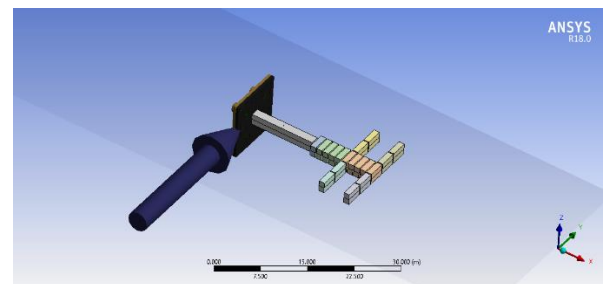

Fig. 38. A depiction of the 135-degree angle wave collision with the multi-hull floating dock in the Time Response solution.
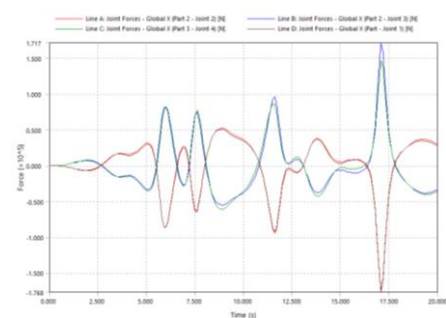

Fig. 39. The force applied to joints 1 to 4 during the collision of a 135-degree angle wave with the multi-hull floating dock in the Time Response solution.
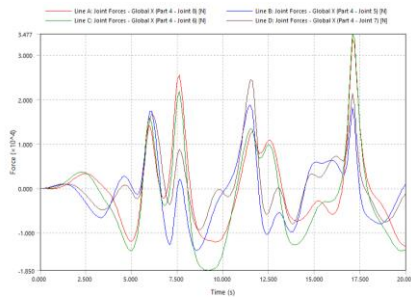

Fig. 40. The force applied to joints 5 to 8 during the collision of a 135-degree angle wave with the multi-hull floating dock in the Time Response solution.

In this situation as well, the highest forces are applied to joints 1 and 2 at the connection points of sections 1 and 2 of the dock.

The results of the analysis of the forces acting on the dock structure and its joints when confronted with a 180-degree incident wave are presented in the figures below.
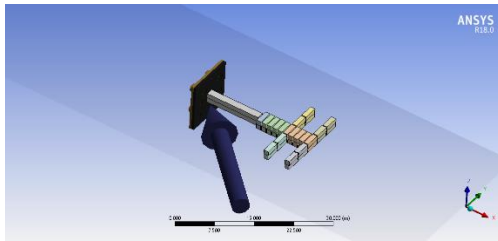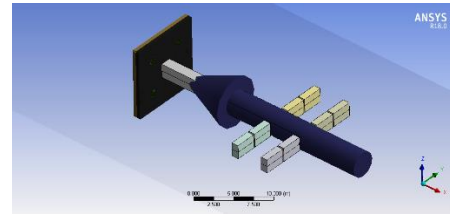

Fig. 41. A depiction of the 180-degree angle wave collision with the multi-hull floating dock in the Time Response solution.
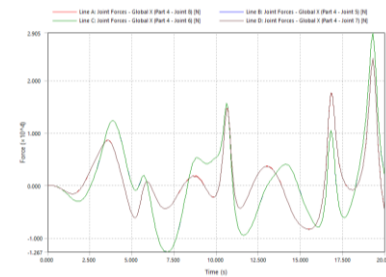
Fig. 42. The force applied to joints 1 to 4 during the collision of a 180-degree angle wave with the multi-hull floating dock in the Time Response solution.
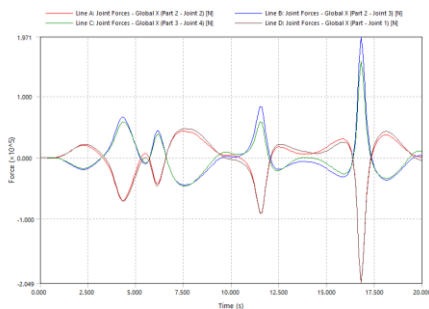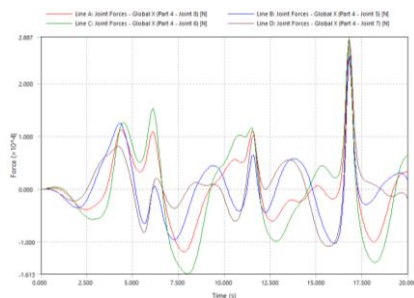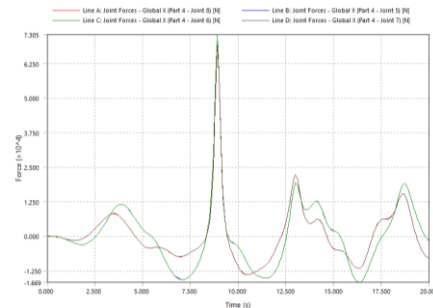

Fig. 43. The force applied to joints 5 to 8 during the collision of a 180-degree angle wave with the multi-hull floating dock in the Time Response solution.
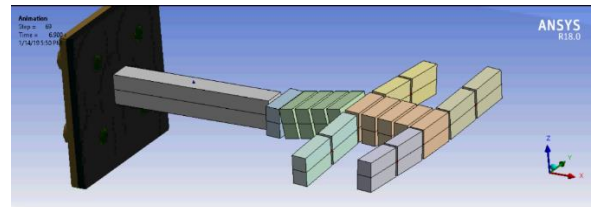
Fig. 44. A view of the maximum deformation of the multi-hull floating dock structure when subjected to wave impact in the Time Response solution.

At the end of this chapter, in order to summarize the results of the Time Response analysis on a multi-body floating dock structure under various wave impacts, the following table is provided:

57

Table. 7. presents the wave characteristics and maximum forces exerted on the connections and body of the multi-body floating dock:

Dock Type	Wave Type	Wave Amplitude	Wave Frequency	Wave Direction	Maximum Force	Force Application Location
Multi-Body	Regular	0.4 m	0.288 Hz	45°	$1.535*10^5$ N	Part 2 - Joint 3
Multi-Body	Regular	0.4 m	0.288 Hz	90°	$-1.768*10^5$ N	Part 1 - Joint 1
						Part 1 - Joint 1
						Part 2 - Joint 2
Multi-Body	Regular	0.4 m	0.288 Hz	135°	$-2.049*10^5$ N	Part 1 - Joint 1
						Part 2 - Joint 2
Multi-Body	Regular	0.4 m	0.288 Hz	180°	$7.305*10^4$ N	Part 4 - Joint 6

3. Analysis of Results:
3.1 Vertical Displacement and Force Distribution

The hydrodynamic analysis revealed notable differences in vertical displacement and force distribution between single-body and multi-pontoon chain floating dock structures.

3.2 Vertical Displacement:

The single-body dock exhibited significant vertical displacement, particularly at connection points, with a maximum displacement of 1.499 meters under head-on wave incidences (Table 4).

In contrast, the multi-section dock model showed reduced vertical motion, with maximum displacements ranging from 0.273 to 1.053 meters under different wave conditions (Table 5).

3.3 Force Distribution:

Forces on the dock structure and joints varied depending on wave direction and incident angle. The highest forces were concentrated at connection points, particularly at the beginning of the dock due to the fixed supports. For instance, under a 45-degree incident wave, the maximum force applied to joints 1 to 4 of the multi-hull dock reached 1.535×10^5 Newtons (Table 7). These findings highlight the advantages of multi-hull configurations in reducing vertical displacement and distributing forces more effectively, improving resilience and performance in maritime environments. Further optimization strategies could enhance the structural integrity and operational efficiency of floating dock systems.

4. Conclusion

This study investigated the hydrodynamic behavior of floating docks, focusing on motion responses of single-hull and multi-hull dock configurations under wave impacts. The three-dimensional diffraction theory method was employed to analyze motion responses, wave forces, and inter-body connection forces through spectral analysis. While most previous studies have modeled docks as continuous rigid structures, this research expanded the scope by examining multi-body dock configurations and their dynamic behavior.

Given the importance of motion responses in floating docks, various parameters such as wave period, incident angle, wave height, and pontoon connection methods were analyzed. The findings confirmed a strong dependence of dock motion on pontoon characteristics and incident wave conditions.

The main conclusions drawn from this research are:

1. Increasing pontoon draft reduces the natural frequency of the structure, while larger drafts result in higher peak response amplitudes.

2. Wider pontoons decrease peak heave motion amplitudes due to increased structural and hydrodynamic mass, which also lowers the natural frequency.

3. Increasing pontoon width reduces peak roll motion amplitude.

4. Exposure to waves of varying periods increases the motion response range of the structure.

5. Multi-hull docks exhibit greater pontoon motions, restricting the operational range.

6. Multi-hull configurations increase heave motions under all four wave directions, particularly with reduced dock dimensions and pontoon weight.

7. Increasing the number of hulls and reducing pontoon length slightly increases roll motion while amplifying peak response amplitudes and natural frequency.

8. Optimal orientation of the dock minimizes environmental loads, ensuring higher efficiency at 0° and 180° wave incidences.

9. Low-stiffness connections lead to discontinuity in vertical displacement and rotation, while increasing stiffness brings multi-hull motion responses closer to single-hull behavior.

10. Connection stiffness influences natural frequency, increasing as stiffness decreases.

11. Higher connection stiffness results in increased joint moments, which peak at lower frequencies.

4.1 Future Research Directions

This study provides a foundation for further scientific advancements in floating dock design and optimization. Key areas for future research include:

1. Optimizing dock dimensions and mooring systems for improved stability and efficiency.

2. Exploring lightweight, durable, and cost-effective materials for pontoons.

3. Enhancing the quality of rigid and flexible connections to optimize floating dock motion.

4. Investigating shore connection methods and analyzing load effects during dock behavior monitoring.

5. References

1- Zhang, J., Ong, M. C., & Wen, X. (2024). Dynamic and structural analyses of floating dock operations considering dock-vessel coupling loads. *Ocean Engineering, 310*(Part 1), Article 118622. https://doi.org/10.1016/j.oceaneng.2024.118622

2- Liang, J. M., Liu, Y., Chen, Y. K., & Li, A. J. (2022). Experimental study on hydrodynamic characteristics of the box-type floating breakwater with different mooring configurations. *Ocean Engineering, 254*, Article 111296. https://doi.org/10.1016/j.oceaneng.2022.111296

3- Gran, V. A., Jiang, Z., & Pan, Z. (2020). Hydrodynamic analysis of floating docks with alternative geometries for floating wind turbine installation. In *Proceedings of the ASME 2020 39th International Conference on Ocean, Offshore and Arctic Engineering* (Vol. 6A: Ocean Engineering, Article V06AT06A057). ASME. https://doi.org/10.1115/OMAE2020-18756

4- Song, J., Imani, H., Yue, J., & Yang, S. (2023). Hydrodynamic characteristics of floating photovoltaic systems under ocean loads. *Journal of Marine Science and Engineering, 11*(9), Article 1813. https://doi.org/10.3390/jmse11091813

5- Al-Sairafi, F. A., Zhang, J., Jiang, C., Almansour, A. I., & Saleh, B. (2024). Enhancing hydrodynamic performance of floating breakwaters using wing plates. *Water, 16*(13), Article 1779. https://doi.org/10.3390/w16131779

6- Wan, C., Niu, Y., Yang, C., & Johanning, L. (2024). Hydrodynamic performance of a hybrid floating power dock combining multi-cantilever type buoys. *Marine Energy Research, 1*(1), Article 10005. https://doi.org/10.70322/mer.2024.10005

7- Li, Y., Ren, N., Li, X., & Ou, J. (2022). Hydrodynamic analysis of a novel modular floating structure system integrated with floating artificial reefs and wave energy converters. *Journal of Marine Science and Engineering, 10*(8), Article 1091. https://doi.org/10.3390/jmse10081091

8- Takeuchi, T., Utsunomiya, T., Gotoh, K., & Sato, I. (2019). Quantitative wear estimation for mooring chain of floating structures and its validation. In *Proceedings of the ASME 2019 38th International Conference on Ocean, Offshore and Arctic Engineering*. ASME. https://doi.org/10.1115/OMAE2019-96750

9- Li, Y. W., Ren, N. X., Cai, W. Y., et al. (2024). Experimental investigation of the hydrodynamic characteristics of a modular floating structure system integrated with WEC-type floating artificial reefs. *China Ocean Engineering, 38*, 1082–1090. https://doi.org/10.1007/s13344-024-0085-z

10- Xu, D. L., Zhang, H. C., Xia, S. Y., et al. (2018). Nonlinear dynamic characteristics of a multi-module floating airport with rigid-flexible connections. *Journal of Hydrodynamics, 30*, 815–827. https://doi.org/10.1007/s42241-018-0089-3

11- Xu, K., Larsen, K., Shao, Y., Zhang, M., Gao, Z., & Moan, T. (2021). Design and comparative analysis of alternative mooring systems for floating wind turbines in shallow water with emphasis on ultimate limit state design. *Ocean Engineering, 219*, Article 108377. https://doi.org/10.1016/j.oceaneng.2020.108377

12- Nazligul, Y. E., & Yazir, D. (2023). Comparison of automated mooring systems against existing mooring systems by using the IF-TOPSIS method. *Ocean Engineering, 285*(Part 2), Article 115269. https://doi.org/10.1016/j.oceaneng.2023.115269

13- Perkovič, M. (2024). Advances in navigability and mooring. *Journal of Marine Science and Engineering, 12*(9), Article 1601. https://doi.org/10.3390/jmse12091601

14- Sirigu, S. A., Bonfanti, M., Begovic, E., Bertorello, C., Dafnakis, P., Giorgi, G., Bracco,

G., & Mattiazzo, G. (2020). Experimental investigation of the mooring system of a wave energy converter in operating and extreme wave conditions. *Journal of Marine Science and Engineering, 8*(3), Article 180. https://doi.org/10.3390/jmse8030180

15- Hennø, E., & Schøyen, H. (2024). A lean approach to comparing the mooring systems of Suezmax tankers. *Journal of Marine Science and Technology, 29*, 956–974. https://doi.org/10.1007/s00773-024-01030-2

16- Ni, X. Y., Cheng, X. M., Wu, B., et al. (2021). Performance analysis of the mooring system of a two-module scientific research and demonstration platform. *Journal of Hydrodynamics, 33*, 901–914. https://doi.org/10.1007/s42241-021-0080-2

17- Samaei, S. R., Hassanabad, M. G., Ghahfarrokhi, M. A., & Ketabdari, M. J. (2021). Numerical and experimental investigation of damage in environmentally-sensitive civil structures using modal strain energy (case study: LPG wharf). *International Journal of Environmental Science and Technology, 18*, 1939–1952. https://doi.org/10.1007/s13762-021-03321-2

18- Samaei, S. R., Azarsina, F., & Ghahferokhi, M. A. (2016). Numerical simulation of floating pontoon breakwater with ANSYS AQWA software and validation of the results with laboratory data. *Bulletin de la Société Royale des Sciences de Liège, 85*, 1487–1499.

19- Samaei, S. R., & Hassanabad, M. G. (2024). The crucial interplay of seas, marine industries, and artificial intelligence in sustainable development. *Eighth International Conference on Technology Development in Oil, Gas, Refining and Petrochemicals.*

20- Samaei, S. R., & Ghodsi Hassanabad, M. (2023). The transformative role of artificial intelligence in engineering sciences with an emphasis on civil engineering and marine industries. *The Second International Conference on Creative Achievements of Architecture, Urban Planning, Civil Engineering and Environment in the Sustainable Development of the Middle East, Mashhad.* Retrieved from https://civilica.com/doc/1893048

21- Samaei, S. R., & Ghodsi Hassanabad, M. (2022). Damage location and intensity detection in tripod jacket substructure of wind turbine using improved modal strain energy and genetic algorithm. *Journal of Structural and Construction Engineering, 9*(4), 182–202. https://doi.org/10.22065/jsce.2021.294103.2488

22- Samaei, S. R., Ghodsi Hassanabad, M., Asadian Ghahfarrokhi, M., & Ketabdari, M. J. (2021). Numerical and experimental study to identify the location and severity of damage at the pier using the improved modal strain energy method—Case study: Pars Asaluyeh LPG export pier. *Journal of Structural and Construction Engineering, 8*(Special Issue 3), 162–179. https://doi.org/10.22065/jsce.2020.246425.2225

23- Samaei, S. R., Ghodsi Hassanabad, M., Asadian Ghahfarrokhi, M., & Ketabdari, M. J. (2020). Structural health monitoring of offshore structures using a modified modal strain energy method (case study: four-leg jacket substructure of an offshore wind turbine). *Journal of Marine Engineering, 16*(32), 119–130.

24- Samaei, S. R., Ghodsi Hassanabad, M., & Karimpor Zahraei, A. (2021). Identification of location and severity of damages in the offshore wind turbine tripod platform by improved modal strain energy method. *Analysis of Structure and Earthquake, 18*(3), 51–62.

25- Samaei, S. R., Ghodsi Hassanabad, M., Asadian Ghahfarrokhi, M., & Ketabdari, M. J. (2021). Investigation of location and severity of damage in four-legged offshore wind turbine stencil infrastructure by improved modal strain energy method. *Analysis of Structure and Earthquake, 17*(3), 79–90